Discover Oncology

RESEARCH Open Access

# Single cell analysis and bioinformatics reveal pyroptosis mechanisms in hepatocellular carcinoma

Wei Luo[1], JunxiaWang[2], Hongfei Wang[3], Fei Liu[1], Taiwei Yang[5], Zhongjun Wu[4*] and Wubin Guo[1*]

*Correspondence:
Zhongjun Wu
wzjtcy@126.com
Wubin Guo
gwb1227@swmu.edu.cn
[1]Department of General Surgery, The Affiliated Traditional Chinese Medicine Hospital, Southwest Medical University, Luzhou, China
[2]Department of Pediatrics, The Affiliated Traditional Chinese Medicine Hospital, Southwest Medical University, Luzhou, China
[3]Department of Pathology, The Affiliated Traditional Chinese Medicine Hospital, Southwest Medical University, Luzhou, China
[4]Department of Hepatobiliary Surgery, The First Affiliated Hospital of Chongqing Medical University, Chongqing, China
[5]Department of General Surgery, Xuyong County Second Name Hospital, Luzhou, China

## Abstract

**Background** Hepatocellular carcinoma (HCC) is the third leading cause of cancer related death, and its molecular mechanisms have not been fully elucidated. This study aims to elucidate the molecular mechanisms linking pyroptosis and immune microenvironment changes in HCC, with a focus on macrophage polarization and inflammatory responses.

**Methods** Selected gene expression profiles from the Gene Expression Omnibus database, established protein-protein interaction (PPI) networks, and performed functional enrichment analysis using databases such as the Kyoto Encyclopedia of Genes and Genomes (KEGG). The expression of relevant hub genes was verified by immunohistochemistry, real-time quantitative PCR, and Western Blot based on clinical tissues. Single-cell identification of HCC cell types and malignant cells, trajectory analysis, and intercellular signal communication further analyzed the molecular mechanisms between immune cells and liver cells. Bioinformatics combined with single-cell analysis to elucidate the immune pyroptosis molecular mechanism that underlay the development of HCC.

**Results** Molecular biology has identified six pyroptosis hub genes in HCC. The key hub genes of immune pyroptosis were validated through immunohistochemistry and in vitro experiments. Enrichment analysis shows that intersecting genes are enriched in immune responses, chemokine mediated signaling pathways, and inflammatory responses. InferCNV and copyKAT accurately predict that malignant cells distribute in HCC tissues, and their main malignant cells may be hepatocytes, endothelium and epithelial cells. Cell trajectory analysis found that monocyte, macrophage polarization could play a first role in HCC. The cellular clustering of single cells revealed the infiltration of immune cells, especially the polarization of macrophages, which plays an important role. Immunohistochemistry suggests that hub genes such as HMGB1, CYCS, GSDMD, IL-1β, NLRP3, and IL18 are the link between macrophage polarization and pyroptosis during HCC development.

**Conclusions** In summary, the main molecular mechanisms underlying the pathogenesis of HCC are related to immune cell infiltration, particularly macrophage infiltration polarization that promotes the secretion of inflammatory factors leading to hepatocyte pyroptosis. These findings provide novel insights into the

macrophage-driven pyroptosis pathways in HCC, potentially paving the way for new immunotherapeutic strategies.

**Keywords** Liver cancer, Macrophages, Pyroptosis, Single-cell analysis

## 1 Introduction

Around the world, hepatocellular carcinoma (HCC) is one of the most common causes of cancer-related deaths. Most patients with HCC are only detected in late stages, which hinders radical treatments such as liver resection and liver transplantation. Due to the delay in treatment, the 5-year survival rate of HCC is only 18% [1–3]. Despite the fact that early discovery is linked to enhanced overall survival. HCC not only seriously damages the physical and mental health of patients, leading to metabolic dysfunction, but also imposes a heavy medical and economic burden on society [4]. Both viral and non-viral factors have been linked to the pathophysiology of HCC. Changes in cellular signaling, persistent inflammation, and tissue remodeling are important contributors leading to HCC regardless of the type of injury [5, 6]. An increasing amount of researches to the commonality of tumor heterogeneity in HCC, which could account for some variations in therapy response and survival outcomes. Therefore, tumor cell heterogeneity plays a key role in its pathogenesis, but its specific pathogenesis is not fully understood [7, 8]. Cell classification of HCC by molecular and cellular characteristics may help guide biomarker discovery and treatment selection. Especially for HCC based on cirrhosis, single-cell technology in HCC [9].

Pyroptosis is a newly discovered program that plays a crucial role in tumor related diseases [10]. At present, most studies believe that cell pyroptosis has a double-edged sword effect on the occurrence and development of liver cancer [11]. Research has shown that cell pyroptosis can induce rapid death of liver cancer cells, thereby reducing the risk of tumor deterioration and metastasis [12]. However, during the process of cell pyroptosis, cellular contents are also released from the interior of liver cells to the exterior, acting as endogenous stimuli to mediate different biological changes in different cells within the liver [13]. Not only that, cells in the liver may also have the potential to undergo or induce pyroptosis in other cells [14]. Therefore, these subsequent biological changes based on cell pyroptosis are also subtly affecting the prognosis of liver cancer [15]. The liver is an important immune organ in the human body, containing immune cells such as liver macrophages, natural killer cells, and cytotoxic T cells [16]. Among them, macrophages in liver tissue and are the first line of defense against cancer cells. Under physiological conditions, liver macrophages are highly susceptible to activation by endotoxins, complement proteins, and other pathogen related molecular patterns through various signaling pathways to exert their phagocytic activity [17]. However, when the NLRP3/Caspase-1 pathway inside hepatic macrophages is activated, it will not only produce pyroptosis by itself but also increase the sensitivity of cells to endotoxin. This process can also cause the body to produce an excessive immune response to aggravate the inflammatory response damage in cancer patients [18].

Pyroptosis is associated with macrophages, cell resistance to pathogens, and transmission to cell, but its role and mechanism in cancer cells are still unclear [19]. Some studies have found that pyroptosis-related risk genes can be used to diagnose HCC, predict the prognosis of HCC, evaluate the infiltration status of immune cells in the tumor

microenvironment, and evaluate the efficacy of immunotherapy-guided immunotherapy [20]. Epicanin (ICT) is a natural compound derived from the dry leaves of the genus Epimedium, with antitumor and immunomodulatory properties. New studies have implicated the caspase1-GSDMD and caspase3-GSDME pathways in pyroptosis triggered by ICT. Moreover, ICT promotes pyroptosis in cocultures of HCC-associated cells and macrophages and regulates the release of inflammatory cytokines and transformation of macrophages into a pro-inflammatory phenotype [21]. Since macrophages monitor the hepatic immune response, their pyroptosis surely upsets the immunological homeostasis of the liver and incites a potent immune response [22]. The process of macrophage pyroptosis results in the active release of pro-inflammatory cytokines such as IL-1β and IL-18. Among these, the pleiotropic pro-inflammatory cytokine IL-1β has the ability to increase the inflammatory response by inducing the release of pro-inflammatory cytokines and drawing neutrophils to liver tissue [23, 24]. Membrane swelling, rupture, and the release of cellular components such as mitochondrial and nuclear DNA, adenosine triphosphate (ATP), high mobility group box-1 (HMGB-1), and pieces of organelles are the results of macrophage pyroptosis. These structures from isolated cells can be identified as Damage Associated Molecular Patterns (DAMPs) once they are discharged into the extracellular environment [25]. Through its interactions with cellular receptors, such as pattern recognition receptors (PRRs), DAMP triggers pro-inflammatory responses. They also cause immunological responses in dendritic and bone marrow cells, which controls the activation of innate immune cells and programmed cell death [24]. These findings imply that the spectrum of immune cell infiltration by macrophage pyroptosis may impact anti-tumor immunity. As a result, HCC and immunological macrophage infiltration are strongly associated. By interfering with macrophage pyroptosis, TME can be changed to prevent tumor cell proliferation and spread. However, more investigation into this intriguing line of inquiry is warranted.

Although many studies have elucidated the role of pyroptosis-related genes in HCC, and more researches have identified the involvement of macrophages in the molecular mechanisms of HCC, few studies have linked macrophage regulation of pyroptosis, especially in the development of HCC. Therefore, the aim of our present study was to clarify the molecular mechanism by which macrophage polarization process regulates pyroptosis leading to HCC occurrence. Bioinformatic analysis based on transcriptome sequencing can screen out the key genes for pyroptosis in the process of HCC development through numerous genes, and initially predict the signaling pathways and biological processes of related genes. Single-cell sequencing-based analysis, on the other hand, can clarify the mechanism of the role of immune cells in the process of HCC and related cells in hepatocarcinogenesis from the cellular direction. Meanwhile, based on single-cell data, trajectory analysis and cell-to-cell communication analysis can provide insights into the relevant roles of various cells. Finally, the joint analysis of predicted pyroptosis genes with single-cell data can reveal the molecular mechanisms of hub genes regulating related cells from a new perspective.

Therefore, in this study, we will use bioinformatic analysis combined with single-cell analysis to systematically elucidate the immune-cell infiltration in the development of HCC, and further clarify the related immune-cell pyroptosis and potential molecular mechanisms of HCC by relevant gene enrichment analysis.

## 2 Materials and methods

### 2.1 Based on bulk RNA material information analysis

#### *2.1.1 Differential gene analysis*

The data set, GSE461 was downloaded from Gene Expression Omnibus (GEO). The gene expression profile of RNA levels in liver cancer tissue and adjacent tissues was measured using the GPL4133 sequencing platform [26]. Used Sangerbox ( version 3.0)'s simple tSEN dimensionality reduction analysis to perform dimensionality reduction grouping on the data [27], and used the "limma" tool for differential gene analysis. The threshold for differential genes was set to the absolute value of log2 fold change | log2FC |>1.2 and P.value < 0.05. Positive numbers indicate upregulation of differentially expressed genes (DEGs). Similarly, | log2FC |<1.2 and P.value < had a value of 0.05, with negative numbers indicating downregulation of DEGs [28, 29]. Used volcano and heatmap to display the results of differential gene expression.

#### *2.1.2 Identification of pyroptosis characteristic genes in HCC*

From literature and MSigDB database, pyroptosis related genes were obtained from the database GSEA | MSigDB (gsea-msigdb.org), and liver cancer pyroptosis characteristic genes were obtained by taking the intersection of pyroptosis genes and GSE46408 differentially expressed genes using the online intersection tool Venny plot [30]. Using the R package survival, we integrated survival time, survival status and gene expression data, assessed the prognostic significance of each gene using the cox method, constructed KM survival curves, and then plotted forest plots using the ggforest function [31, 32]. In order to further discover prognostic genes for HCC, forest pattern maps were used for predicting pyroptosis related genes. Finally, the intersection of pyroptosis characteristic genes in HCC and pyroptosis related genes in forest pattern maps was taken to obtain the pyroptosis hub genes involved in HCC [33, 34]. Enrichment analysis of pyroptosis hub genes in HCC using KEGG and Reactome to explore the potential molecular mechanisms underlying its pathogenesis [34–36].

#### *2.1.3 Construction of a hub gene network for HCC*

PPI network analysis was carried out on the pyroptosis hub genes implicated in HCC of species, which was limited to Homo sapiens with a confidence level > 0.4, using a string database ( http://string-db.org/ Cytoscape (version 3.9.1) was used to build the PPI ne twork [37, 38]. To determine the interactions between the important apoptotic genes involved in the development of HCC, use the co expression analysis module of the string database. Lastly, export these genes' molecular 3D structures from the string database for further verification.

### 2.2 Single cell analysis based on ScRNAseq

#### *2.2.1 Data preprocessing*

The sample data was downloaded from the GEO database, and this analysis included 2 cases of liver cancer tissue from dataset GSE125449 and 2 cases of normal liver tissue from dataset GSE136103 [39, 40]. All data processing was done using BioBean (Zhejiang ICP No. 2023020822) (Sheng-Xin-Dou-Ya-Cai) sprout analysis tools, (Sheng-Xin-Dou-Ya-Cai) sprout analysis tools, an online analysis software and platform for single-cell analysis. After obtaining the data, select the single-cell analysis tool and import 10 x

genomics data. This tool uses the Percentage Feature Set function in the Seurat package of R language to calculate mitochondrial content and rRNA content, and analyzes the relationship between mitochondrial content and ncount (UMI), nFeature (number of genes) through correlation analysis. The mitochondrial content is set within 10%, the nFeature number is within 4000, and the dimensional reduction PC value is 10. After data quality control, there are still many miscellaneous cells and excess cell fragments. Set cell filtering criteria based on quality control data. Based on the tsne/UMAP map of the distribution of each sample cell after cell filtration, the Harmony tool for batch processing was selected [41].

#### *2.2.2 Cell clustering and annotation*

To use principal component analysis (PCA) for dimensionality reduction, we employed 2000 highly variable genes. Then use Seurat's random neighbor embedding (t-SNE) algorithm, the "FindNeighbors" and "FindClusters" (resolution = 0.1) functions to select the best cluster for visualization. Finally, the "SingleR" package, marker gene markers, and literature review were used to annotate cells from different subgroups.

After the first clustering, it was found that there were several types of cell populations with insufficient clustering and several identical feature groups. Therefore, these special cell populations were extracted again for secondary subgroup analysis and definition. The best clusters was selected for visualization using the Seurat's random neighbor embedding (t-SNE) algorithm, "FindNeighbors" and "FindClusters" (resolution = 0.1) functions. Finally, the "SingleR" package combined with literature search to annotate the cells of the subpopulation.

#### *2.2.3 Identification of malignant cells in HCC*

The microenvironment of tumors is made up of both malignant and non-malignant cells, and malignant cells usually have widespread chromosomal abnormalities. To find evidence of extensive chromosomal copy number changes in somatic cells, such as the addition or deletion of large chromosomal segments or complete chromosomes, InferCNV is utilized to examine tumor scRNA data [42]. InferCNV infers chromosomal variations by comparing gene expression intensity at different locations of the tumor genome with a set of reference normal cells. Like inferCNV, CopyKAT is a technique for inferring tumor cell CNV. The idea is also to use single-cell transcriptome data to deduce a cell's chromosome ploidy, which allows one to determine if the cell is diploid or aneuploid—that is, whether it is a tumor or a normal cell [43]. This time, InferCNV and copyKAT were used to identify malignant cells in the sample tissue and assess the degree of tissue malignancy. The single cell expression matrix file, cell type file, and gene location information file on chromosome were obtained after preliminary single cell clustering screening. InferCNV analysis was performed by gene filtering, logarithmic transformation, centrocyte setting and adjusting the reference cells after importing the three files into the online analysis tool. Similarly, after importing the parameter files, copyKAT firstly normalized the gene expression and stabilized its variance, automatically found diploid cells as normal cells, and for each abnormal cell, used MCMC to find its CNV breakpoints and obtained segments. finally, the copyKAT results were obtained.

#### 2.2.4 Analysis of cell development trajectory

Single cell pseudo temporal analysis is an analytical tool used to study single-cell RNA Seq data, revealing cellular heterogeneity, function, and developmental processes. Monocle 2 uses a simple, unbiased, and highly scalable statistical program to select cell populations with trajectory progression characteristics [44]. Then, it employed a class of manifold learning algorithms aimed at embedding a main image in high-dimensional single-cell RNA seq data. The selected cells for secondary clustering are mapped according to their cell types, with each point representing a cell. Pseudotime represents the calculated developmental time, with smaller values indicating that the cell is at the beginning of development and larger values indicating that the cell is closer to the end of development. State represents the developmental status of cells, with smaller values indicating early development. Similarly, after clustering, the obtained expression matrix file, cell type file, and gene location information file on chromosomes were imported, genes related to biological processes were identified by Monocle 2's R package, differentially expressed genes were selected, MST was constructed with DDRTree, cells were projected onto MST, and pseudo-times were calculated recursively by MST.

CytoTACE is a tool for inferring cell differentiation trajectories based on single-cell expression matrices. CytoTACE packages are used for secondary clustering and cell trajectory analysis. Here, a CytoTACE score is calculated to measure the state of cell differentiation. In addition, CytoTracy can further label target genes in cells at different developmental stages, thus selecting the key apoptotic genes involved in the development of HCC for trajectory prediction.

#### 2.2.5 Cell to cell communication

In multicellular organisms, communication between cells is frequently facilitated by cytokines and membrane proteins, which serve to control biological activity and maintain the organism's effective and organized functioning. Among these, intercellular communication mediated by receptor ligands is essential for coordinating a range of biological activities, including illness, differentiation, and development. Cell communication analysis infers the interactions between different cells by analyzing the expression and pairing of receptors and ligands in different cell types. The sample data were downloaded from the GEO database, and the dataset for this communication was two liver cancer tissues in GSE125449 and two normal liver tissues in GSE136103.Used bioinformatics bean sprouts cell communication analysis function for cell communication analysis of HCC. Finally, the communication signals between the important cells were selected for the analysis [45].

#### 2.2.6 Joint analysis of bioinformatics and single-cell sequencing

Single cell technology can not only identify specific cell types present in different tissues, but also further identify the expression of different regulatory factors and target genes in different cells. Based on transcriptome sequencing, the key apoptotic genes involved in HCC were obtained and analyzed in combination with single cells to further validate the expression and potential molecular mechanisms of related genes in different cells. Using single-cell analysis tools, the distribution of different cell types in different sample tissues was at first identified. Secondly, the different cell distributions and expression levels of the focal pyroptosis genes involved in the occurrence of HCC in secondary clustering

were identified. R language package was used to draw UMAP and violin expression maps of specific gene expression. Human Protein Expression Profile (THPA) Database (https://www.proteinatlas.org/) We summarized and aggregated the expression of com mon human proteins in different tissues and cells, and searched for the key apoptotic genes involved in HCC in this database to obtain the expression of related proteins in liver cancer tissues and cells, further verifying our specific gene expression results [46].

#### *2.2.7 Validation of core genes in clinical samples*

To validate the aforementioned analysis results, we obtained consent from the patients and their families, and received approval from the Ethics Committee of the Affiliated Traditional Chinese Medicine Hospital of Southwest Medical University (Nos. YJ-KY2024048). During the surgery, we collected cancerous and adjacent non-cancerous tissues from the patients. The exclusion criteria were as follows: (1) history of radiotherapy or chemotherapy; (2) diabetes or cardiovascular diseases; (3) patients who declined to comply with the study protocol. Prior to use, each sample was rapidly stored in liquid nitrogen. The ages of the patients ranged from 42 to 63 years, with a mean age of 50.4 years. The male-to-female ratio was 1:1, and the relevant tumor staging and survival information are presented in Supplementary Table S1.

#### *2.2.8 Immunohistochemistry (IHC) staining*

The sections were hydrated with gradient ethanol and dewaxed with xylene. Subsequently, the slides were treated with hydrogen peroxide to inhibit endogenous peroxidase activity, and goat serum was used to prevent nonspecific binding sites. After that, the proper volume of primary antibody was added, and it was kept at 4 °C for the entire night. The samples were stained with diaminobenzidine and counterstained with hematoxylin on the second day after being treated for 30 min at room temperature with the secondary and tertiary antibodies. After that, pictures stained with immunohistochemistry were captured using an upright microscope. Primary and secondary antibodies were obtained from Thermo Fisher Scientific, located in China. The primary antibody is diluted with diluent at a ratio of 1:500, and the corresponding secondary antibody is diluted at a ratio of 1:1000. Impact Acquisition with Leica DM3000 & DM3000 LED Biomicroscope.

#### *2.2.9 Real-time quantitative PCR analysis*

Sangon Biotech was responsible for the design and synthesis of gene primer sequences (Sangon Biotech, China). Primer sequences for each gene are listed in Table 1. Total RNA was extracted using an RNA extraction kit (#AM2071; InvitrogenTM) following tissue homogenization. Complementary DNA was obtained using a Primary QuickScript™

**Table 1** The primer sequences used for PCR amplification

| Gene | Forward primer sequence | Revere primer sequence |
|---|---|---|
| HMGB1 | CGGACAAGGCCCGTTATGAA | GAGGAAGAAGGCCGAAGGA |
| CYCS | ATCTGGGGAGAGGATACACTG | AAGTCTGCCCTTTCTTCCTTC |
| GSDMD | GATGGGCAGATACAGGGCAG | CCAGGTGTTAGGGTCCACAC |
| IL1B | CCAGGGACAGGATATGGAGCA | TTCAACACGCAGGACAGGTA |
| NLRP3 | GATCTTCGCTGCGATCAACA | GGGATTCGAAACACGTGCATT |
| IL18 | GACCAAGTTCTCTTCATTGACC | AGATAGTTACAGCCATACCTC |
| GAPDH | GCACCGTCAAGGCTGAGAAC | TGGTGAAGACGCCAGTGGA |

RT Reagent Kit with gDNA Eraser (#AM2071; Invitrogen). SYBR Green qPCR mix (#A46012; Applied Biosystems) was used forRT-qPCR on a 7500 Real-Time PCR System (Thermo Fisher Scientific, Waltham, MA, USA) for 40 cycles. GAPDH was used as the reference gene, and the relative expression levels of each gene compared to GAPDH were calculated using the $2^{-\Delta\Delta CT}$ method.

#### *2.2.10 Western blot*

Following three rounds of cold phosphate-buffered saline (PBS) washing for each batch of samples, tissues were pulverized in liquid nitrogen and proteins were extracted using high-efficiency RIPA lysis buffer (R0010, Solarbio). With a BCA protein assay kit (PC0020, Solarbio), the total protein content was determined. After that, the samples were heated for five minutes at 95 °C to denature the proteins. After being separated using 10% SDS-PAGE, a 20 μg protein sample was transferred to a PVDF membrane. The membrane was incubated in non-fat milk for 1 h to block nonspecific binding, followed by overnight incubation at 4 °C with primary antibodies against NLRP3 (IMMUNOWAY, 1:800, Item No. MA5-32255), IL18 (IMMUNOWAY, 1:1000, Item No.PA5-79477), GSDMD (IMMUNOWAY, 1:800, Item No. PA5-116815), IL-1β (IMMUNOWAY, 1:1200, Item No. P420B), CYCS (IMMUNOWAY, 1:800, Item No. MA5-11674), HMGB1 (IMMUNOWAY, 1:1000, Item No. MA5-17278), and GAPDH (IMMUNOWAY, 1:5000, Item No. 39-8600). Subsequently, they were incubated with the corresponding secondary antibodies. All antibodies were purchased from Thermo Fisher. Chemiluminescent substrates (Invitrogen) were used to visualize the immunoblots, and quantification was performed using Image Lab 3.0 software.

### 2.3 Statistical analysis

GraphPad Prism 9.0 was used for the statistical analysis. The data are shown as histograms of the means from three or more separate experiments, plus or minus the standard error of the mean (SEM) values. The t-test was used to compare two groups when the samples were normally distributed; non-parametric tests were used in other cases. ANOVA was utilized to compare samples from several groups in a one-way fashion. The Tukey method was utilized to conduct comparisons between the two groups; a statistically significant result is indicated by $^{*}P < 0.05$, and a high level of significance is indicated by $^{**}P < 0.01$.

### 2.4 Result

#### *2.4.1 Results of differential gene analysis based on different groups*

After extracting sample data from the GEO dataset, 12 specimens, 6 liver cancer tissues, and 6 adjacent tissues were included. The gene expression profiles of the sample tissues are presented in Supplementary Table S2. Simple tSEN dimensionality reduction analysis showed significant differentiation between HCC samples and adjacent samples, which is instructive for the identification of pyroptosis-related differential genes in HCC (Fig. 1A). 4725 DEGs were found among 19,712 genes in the study comparing cancer samples to control samples, with 3943 genes being upregulated and 782 genes being downregulated (Supplementary Table S3, Fig. 1B, C).

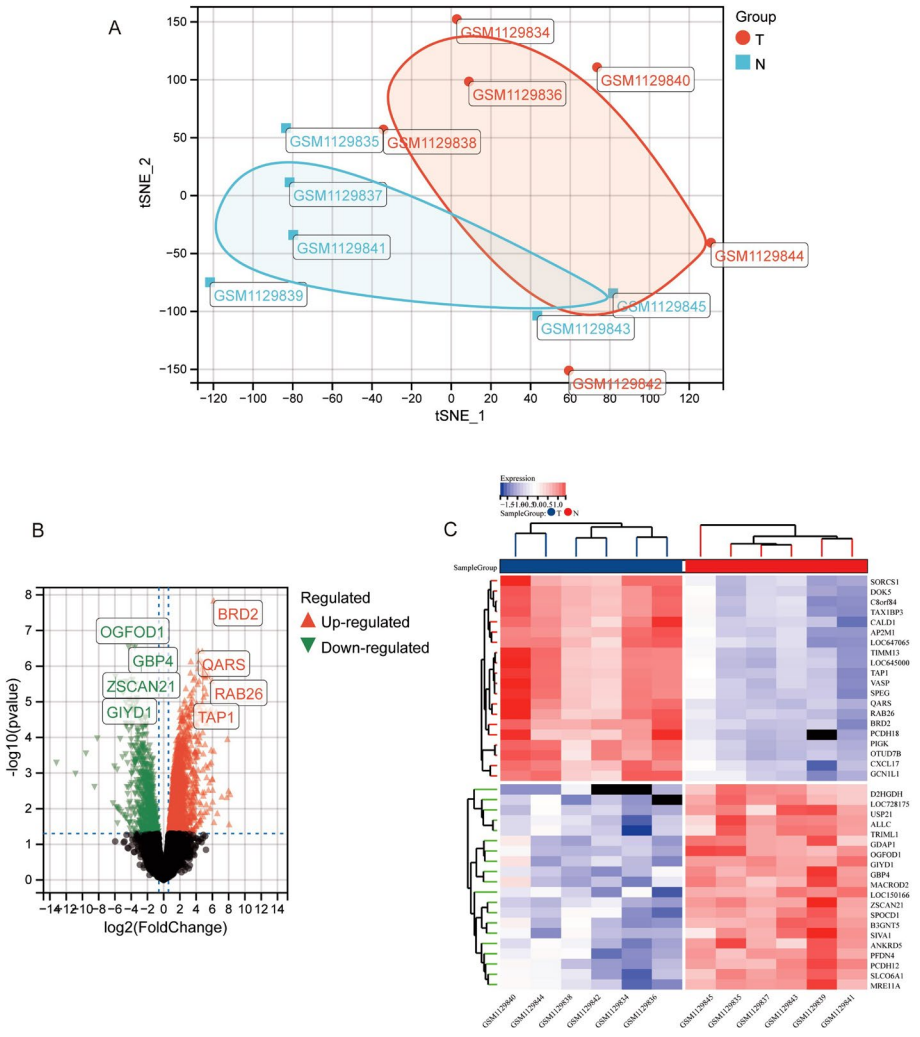


**Fig. 1** Limma differential analysis: **A** Simple tSEN dimensionality reduction analysis shows significant differences between liver cancer samples and adjacent samples. **B** Volcanic map of differentially expressed genes in GSE46408 samples, with green triangles indicating downregulated genes and red triangles indicating up-regulated genes, and black origins indicating no significantly different genes. **C** Heat map of differentially expressed genes in GSE446408 samples, with blue indicating downregulation and red indicating upregulation

### 2.5 Screening of genes with characteristic features of pyroptosis

57 genes related to cell pyroptosis were obtained from literature and MSigDB database (Supplementary Table S4). The intersection of cell pyroptosis related genes and GSE46408 sample tissue differentially expressed genes was obtained through Venny plot, resulting in 17 intersecting pyroptosis characteristic genes (Fig. 2A). Forest pattern analysis further screened 15 genes related to pyroptosis, which has a certain effect on the prognosis of liver cancer (Supplementary Table S5, Fig. 2B, C). Finally, the genes in the forest pattern map were intersected with the genes associated with liver cancer necrosis, resulting in significant liver cancer necrosis hub genes (Supplementary Table S6, Fig. 2D). The KEGG results showed that the occurrence of liver cancer is closely related to signaling pathways such as Necroptosis, Cytosolic DNA sensing pathway, Pyroptosis multiple species, Hematotoxic cell line, NF kappa B signaling pathway, Autophagy animal, Hepatis C, Hepatis B, MAPK signaling pathway, and pathways in cancer. The results

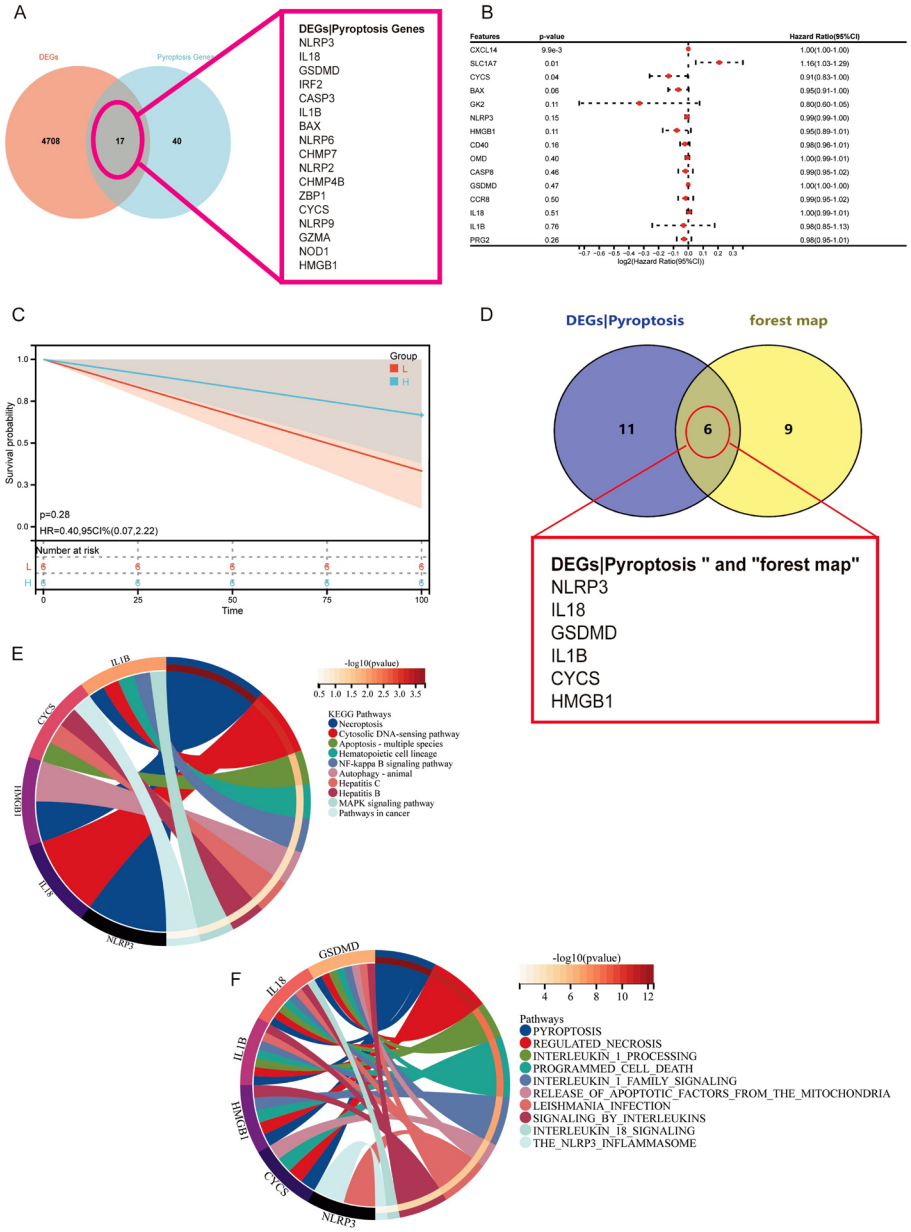


**Fig. 2** Characteristics of gene apoptosis: **A** intersection diagram of differentially expressed genes and cell pyroptosis genes in GSE46408 sample tissues. **B** Forest pattern diagram of pyroptosis related genes in GSE46408 sample tissues. **C** K-M survival curve of forest pattern prediction diagram. **D** Intersection of genes and pyroptosis characteristic genes in forest pattern diagram, KEGG analysis chord diagram of E-junction pyroptosis genes, F. Reaction analysis chord diagram of junction pyroptosis genes

of the Reactome showed that the occurrence of liver cancer was closely associated with signaling pathways such as.

Pyroptosis, Regulated Necrosis, Interleukin 1-Processing, Programmed Ceekk deATH, Interleukin 1-Family Signaling, Signaling-Byinterleukins, Interleukin-18-Signaling, and The-NLRP3-Inflammasome (Fig. 2E, F).

### 2.6 Protein analysis of liver cancer necrosis hub genes

By taking the intersection of genes in the forest model map and the characteristic genes of liver cancer necrosis, six significant liver cancer necrosis hub genes were obtained,

including NLRP3, IL18, GSDMD, IL-1β, CYCS, and HMGB1. To clarify the potential association of six genes, a protein-protein interaction network diagram was constructed using PPI (Fig. 3A). The results showed that the six hub genes were closely related, and further co expression analysis showed that GSDMD, IL18, NLRP3, and HMGB1 were significantly co expressed in the hub genes (Fig. 3B). Based on this, we downloaded the 3D pattern structure diagrams of these four hub genes (Fig. 3C-F). The pattern diagram shows the chemical molecular structure of the relevant hub genes, which is instructive for the subsequent study of in-depth protein target or treatment point. This could also provide direction for subsequent studies.

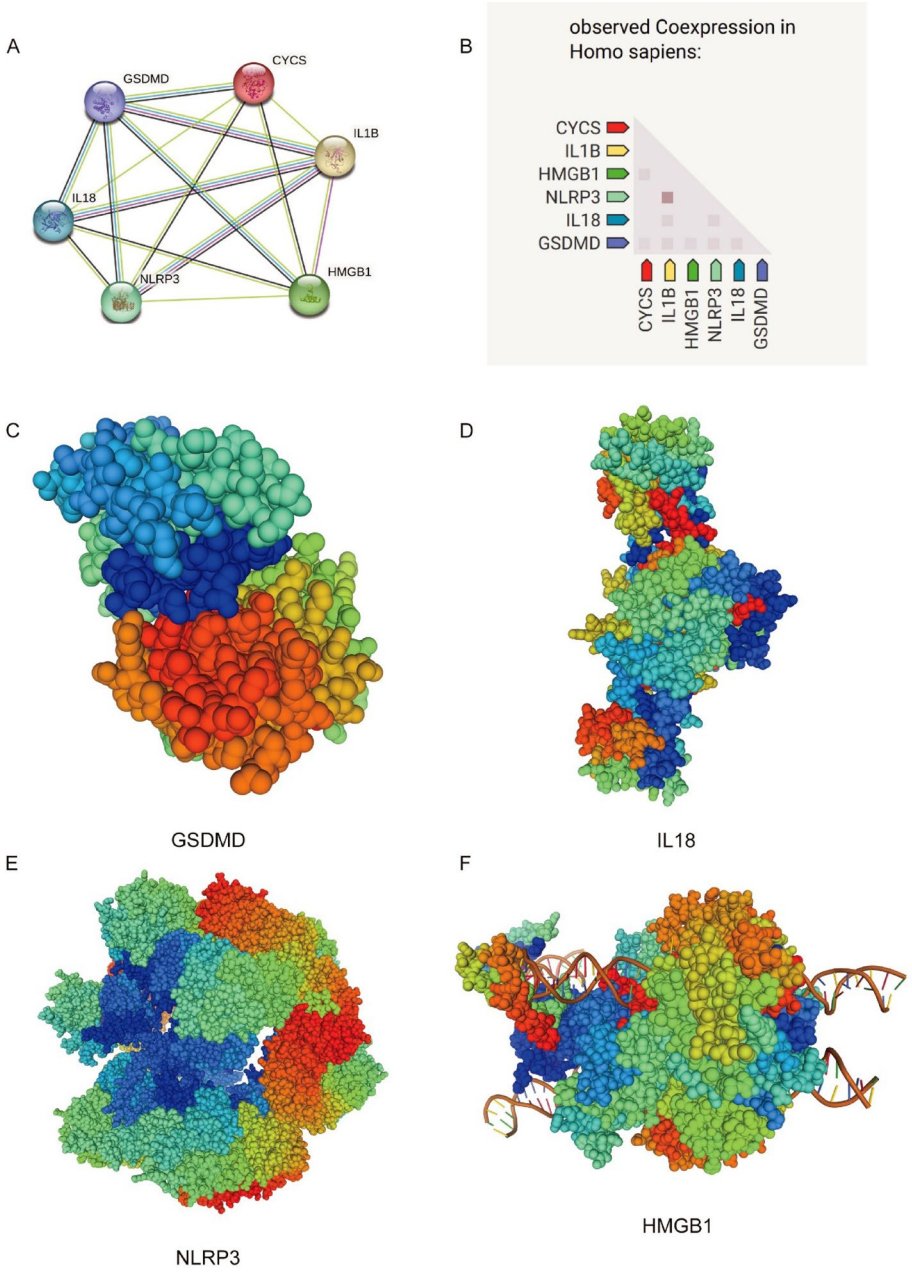


**Fig. 3** Protein analysis of liver cancer necrosis hub genes: **A** Hub gene protein mapping, **B** Hub gene co expression pattern diagram, **C** 3D structural pattern diagram of GSDMD, **D** 3D structural pattern diagram of IL18, **E** NLRP3 3D structural pattern diagram, **F** 3D structural pattern diagram of HMGB1

#### *2.6.1 Grouping and definition of single cells*

After preliminary processing of single-cell sample data, both the expression point map and violin plot of cell RNA suggest the need for further cell filtration (Fig S1). Set nFeature-RNA and nCount-RNA to be less than 4000, percent.mt and percent.Ribo to be less than 0.1, select 10 PCs, and use the Harmony batch removal tool to remove miscellaneous cells and excess cell debris. After filtering, the miscellaneous cells and excess cell debris are effectively removed (Figure S2).

By using the R language package to perform marker gene labeling on single-cell data after batch removal, we obtained the marker genes for all cells (Supplementary Table S7). Through marker gene classification, we obtained 11 cell subgroups. Using the singleR package combined with literature search to classify subgroups, the distribution of marker genes in different cell populations was marked along the linear tree axis, and the TOP5 marker gene point maps showed the significantly expressed genes in different subgroups (Fig. 4A, B). Based on singleR and TOP5 marker genes, we define the distribution of cell populations from 0 to 10 as NK_cell, Monocyte, T-cell: CD4+_ effector_memory, Hepatocytes, Endothelialcells, Tissue_stem-cells, B-cell, Epithelialcells, Hepatocytes, T-cell: gamma delta, Hepatocytes (Fig. 4C, D). Among them, the 0 cell group significantly aggregated and had a large number of cells, while group 1 aggregated 4 tissue samples. Groups 3, 8, and 10 were all defined as Hepatocytes. Therefore, we extracted these cell groups again for secondary clustering analysis. After the secondary cell clustering definition, the UMAP plot showed that a total of 8 cell subgroups were clustered, and based on singleR and TOP5 marker genes, subgroups 0 to 7 were defined as macrophage M1, macrophage M0, Hepatocytes, Hepatocytes, Monocyte, Hepatocytes, macrophage M2, and Hepatocytes, respectively (Fig. 4E, F).

### 2.7 Identification of malignant cells

Cancer tissue is often deformed due to infiltration of malignant cells, so we believe that the number of malignant cells in liver cancer tissue is increasing. We preliminarily believe that the UMAP distribution cells in the two liver cancer samples have a higher proportion of malignant cells. Therefore, we used InferCNV and copyKAT to identify malignant cells in the sample tissues (Fig. 5A). Group 0 NK cells belong to normal sample tissue cells, and the UMAP plot shows no significant infiltration of other tissue sample cells in Group 0. Therefore, we used Group 0 cells as normal reference cells for InferCNV analysis. The InferCNV plot showed that all other cell subsets exhibited malignant lesions (Fig. 5B). Further copyKAT analysis accurately identified the significant expression of malignant cells in two liver cancer tissue samples, and the cell grouping UMAP map showed that these malignant cells may be Hepatocytes, Endothelial cells, and Epithelial cells (Fig. 5C-E). Therefore, InferCNV and copyKAT accurately predicted the distribution of malignant cells in liver cancer tissues, and the main malignant cells may be liver cells, endothelial cells, and epithelial cells.

#### *2.7.1 Cell trajectory analysis*

Based on the analysis of single-cell secondary atlas definition, immune cells such as 0, 1, 4, and 6 play an important role in the occurrence and progression of liver cancer. We conducted cell trajectory analysis on these immune cells. In Fig. 6A, the black dots represent differentially expressed genes selected based on the classification of four cell

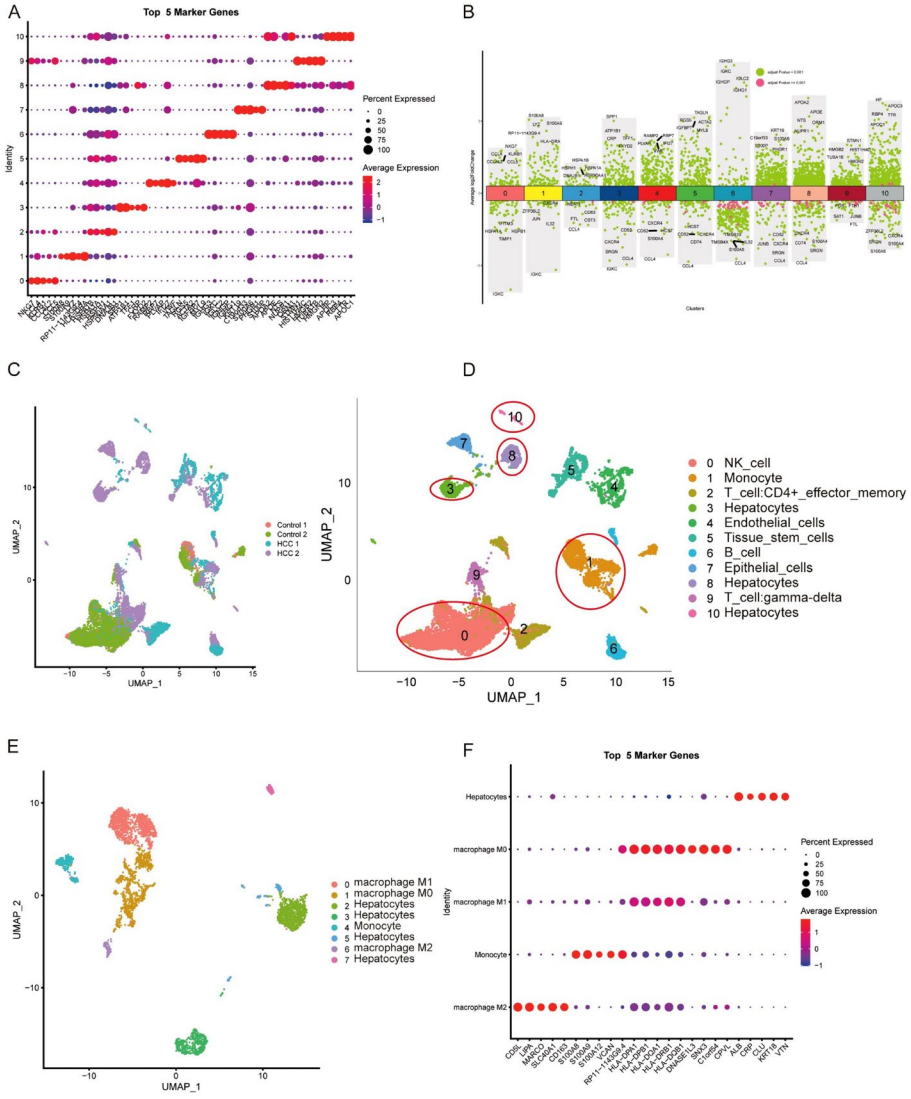


**Fig. 4** Cell Grouping: **A** Single cell marker gene TOP5 significantly expressed gene point map, **B** Single cell marker gene distribution tree map, **C** Single cell UMAP sample tissue distribution, **D** Single cell sample grouping UMAP map, **E** Secondary clustering sample grouping UMAP map, **F** Secondary clustering sample marker gene TOP5 significantly expressed gene point map

populations and used for subsequent monocle 2 analysis; Fig. 6B shows the tsne plot of cell clustering distribution in principal components, where different colors represent branches with different cell fates. Group 1 in red represents macrophage M1, green represents macrophage M0, light blue represents monocytes, and purple represents macrophage M0; In the survival state diagram of cell clustering distribution, value 1 represents the early developmental stage, and value 3 represents the late developmental stage (Fig. 6C). In the time-series diagram of cell clustering distribution, the intensity of colors indicates the sorting of cells based on pseudo time values. Time series analysis revealed that monocytes are early developing cells that gradually develop into macrophages over time, and then differentiate into M1 and M2 macrophages. This developmental process is consistent with the developmental trajectory of monocytes/macrophages, indicating that the pseudo temporal analysis of monocyte 2 is correct (Fig. 6D). In addition, to validate the liver cancer necrosis hub genes identified through bioinformatics analysis,

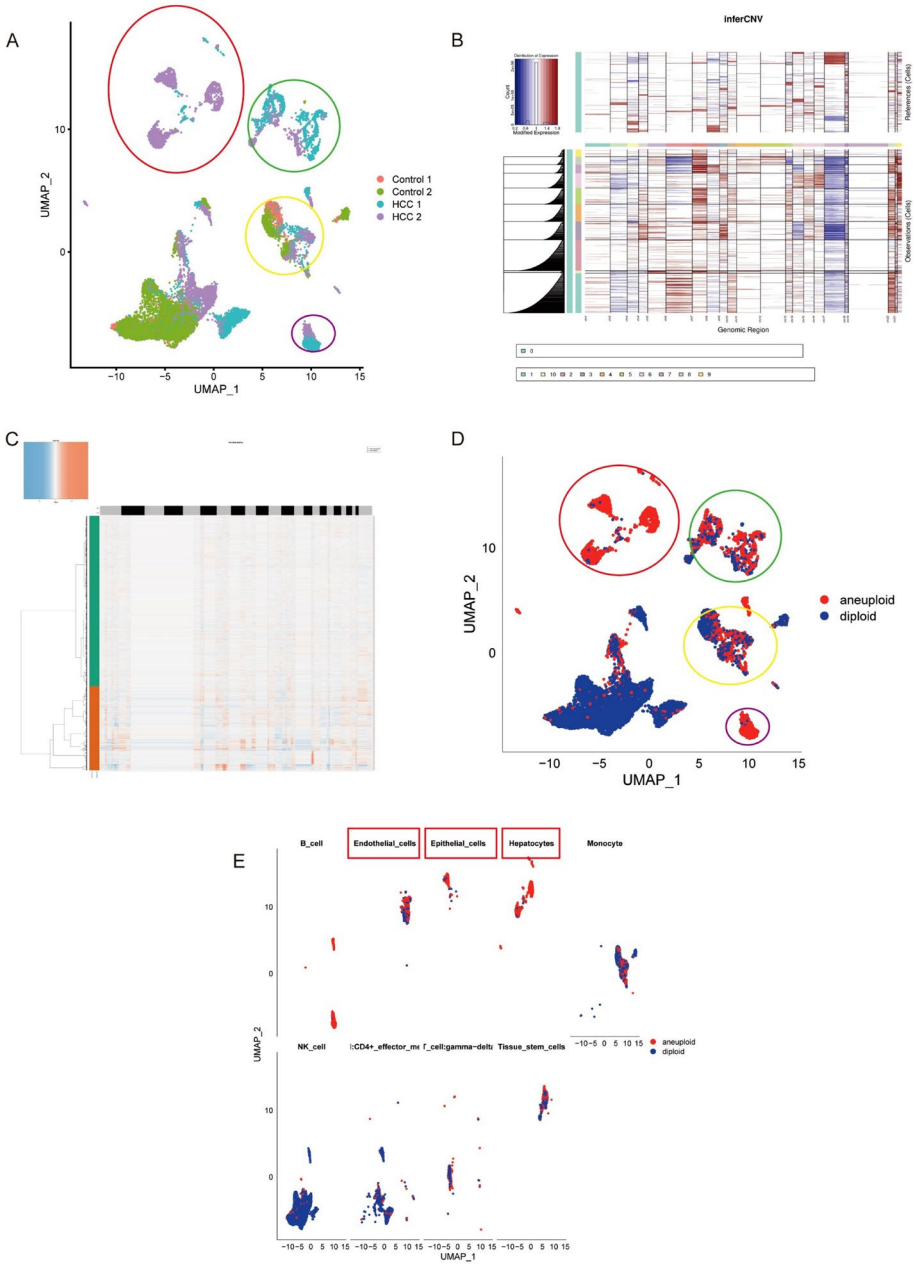


**Fig. 5** Identification of malignant cells: **A** distribution of single-cell samples in different tissues, with circles indicating possible malignant cells, **B** InferCNV malignant cell prediction results, 0 cells indicating normal cells, and the rest of the cell population showing malignant lesions. **C** copyKAT malignant cell prediction heatmap, **D** CopyKAT malignant cell prediction UMAP map, with red circles representing malignant cells and blue circles representing normal cells. The data shows that malignant cells are mainly expressed in two cases of liver cancer tissues. **E** The cell grouping of malignant cells shows that these malignant cells may be Hepatocytes Endothelial_cells、Epithelial_cells

we conducted CytoTracy trajectory analysis. The results showed that these genes were significantly expressed in all four cell populations. Among them, HMGB1, CYCS, and GSMDM are positively correlated, while IL-1β, IL18, and NRRP3 are negatively correlated (Fig. 6E). We can infer from the proportion of cell clusters and the developmental trajectory of monocytes 2 that the light blue cell cluster in the upper left corner of the CytoTracy diagram is monocytes, the yellow cell cluster in the middle is M0 macrophages, the light red cell cluster in the upper right corner is M1 macrophages, and the

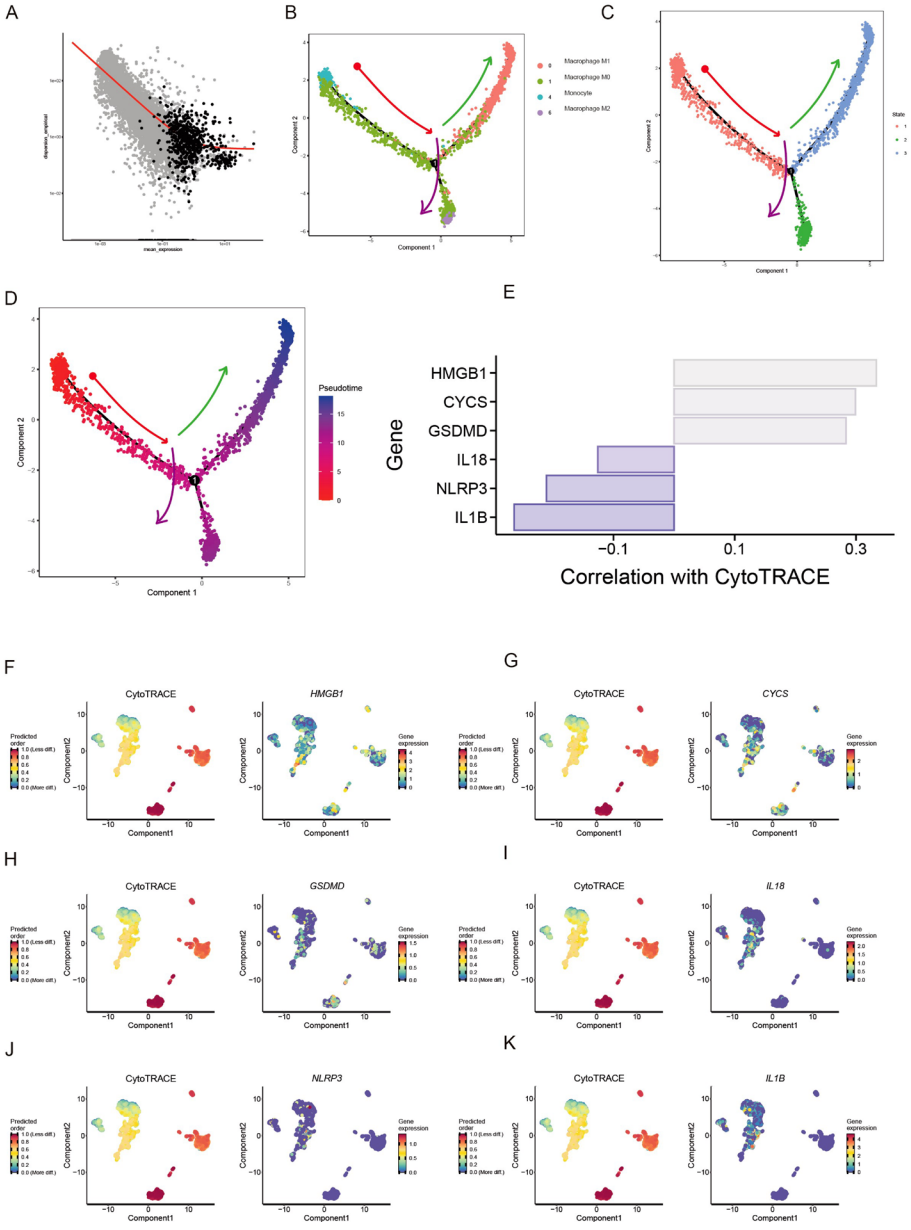


**Fig. 6** Cell Trajectory Analysis: **A** scatter plot of pseudo temporal analysis data screening, **B** principal component expression plot of pseudo temporal analysis, **C** survival status plot of pseudo temporal analysis, **D** temporal developmental trajectory plot of pseudo temporal analysis, **E** expression correlation values of pyroptosis hub genes in CytoTRACE trajectory analysis, **F** CytoTRACE trajectory expression plot of HMGB1, **G** CytoTRACE trajectory expression plot of CYCS, **H** CytoTRACE trajectory expression plot of GSDMD, **I** IL18 CytoTRACE trajectory expression plot, **J** NLRP3 CytoTRACE trajectory expression plot, **K** IL-1β CytoTRACE trajectory expression plot.'

dark red cell cluster in the lower right corner is M2 macrophages. The CytoTracy trajectory of HMGB1 shows that it is mainly distributed in M0 macrophages, while the CytoTracy trajectory of CYCS shows that it is mainly distributed in M0 macrophages and M2 macrophages. The CytoTracy trajectories of GSDMD are mainly distributed in M2 macrophages, IL-1β are mainly distributed in M0 macrophages, IL18 are mainly distributed in monocytes, M0 macrophages, and NRRP3 are mainly distributed in M0 macrophages (Fig. 6F-K). Collectively, these results indicate that focal death hub genes are involved in the regulation of various immune cells, especially macrophage polarization processes.

Therefore, we believe that the link between macrophages and pyroptosis genes is a new direction for the development and prognosis of HCC.

### *2.7.2 Analysis of intercellular communication in cells*

Inter cellular communication provides us with assistance in understanding the interactions between different cells. Figure 7A shows the communication connections between all cell populations, while Fig. 7B shows the communication connections between each type of cell population and other cells. The thicker the line, the tighter the communication between cells. From Fig. 7B, it can be seen that the communication connections between cell populations 4, 5, 7, and 8 are relatively close, and these cells correspond

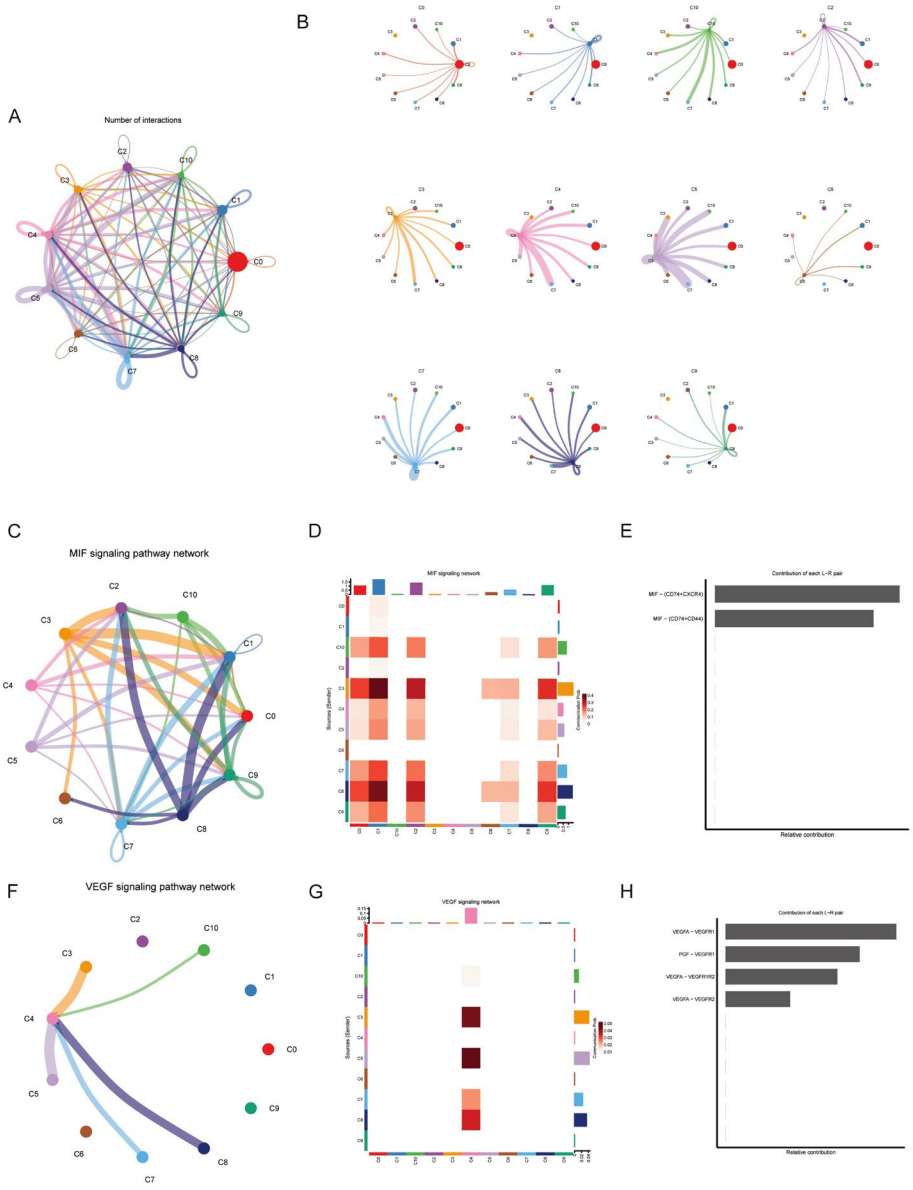


**Fig. 7** Cell communication analysis: **A** all intercellular communication diagrams of cell subpopulations, **B** communication connections between different cell subpopulations and other cells, **C** MIF signaling pathway network, **D** MIF signaling pathway network heatmap, **E** MIF signaling pathway network receptor information, **F** VEGF signaling pathway network, **G** VEGF signaling pathway network heatmap, **H** VEGF signaling pathway network receptor information

exactly to Hepatocytes, Endotheliales, Epitheliales, and Tissue stem cells. Therefore, we found that the communication between these malignant cells exacerbates the occurrence of liver cancer. Further exploration of the MIF signaling pathway network and VEGF signaling pathway network revealed the potential mechanisms underlying their malignant transformation. The MIF signaling pathway network showed significant communication between C3 and C8 Hepatocytes and C0 NK cells, C1 monocytes, and C2 T cells (Fig. 7C, D). According to ligand information, CD74 is the main marker of macrophage migration inhibitory factor. Furthermore, we discovered that the two ligand receptor pairings (L-R pairs) that have the greatest influence on the MIF signaling pathway are MIF - (CD74 + CXCR4) and MIF - (CD74 + CD44). Tumor cells exhibited a considerable increase in the expression of receptors CXCR4 and CD74, suggesting that the MIF signaling pathway is activated in malignancies (Fig. 7E). The VEGF signaling pathway network showed C4 Endothelial cells and C3 Hepatocytes, C5 Tissue Stem Cells, C7 Epithelial Cells, and C8 Hepatocytes have strong communication, and VEGF - (VEGFA + VEGFR) is the ligand receptor pair (L-R pair) that contributes the most to the MIF signaling pathway, indicating that the VEGF signaling pathway is activated in tumors (Fig. 7F-H).

#### *2.7.3 Bioinformatics and single cell combined analysis*

The distribution maps of different cells in different sample tissues show that NK cells and monocytes are mainly distributed in normal liver tissue, Hepatocytes, Endothelial cells, Epithelial cells, and Tissue stem cells are mainly distributed in liver cancer tissues (Fig. 8A, B). Based on the secondary clustering distribution and violin plot of six hub genes, HMGB1, CYCS, and GSDMD were significantly expressed in all cell populations from 0 to 7, while IL-1β and NLRP3 were mainly expressed in monocytes, M0 macrophages, M1 macrophages, M2 macrophages, and IL18 was mainly expressed in monocytes and M0 macrophages (Fig. 8C-I). In summary, inflammatory factors such as IL-1β, NLRP3, and IL18 are mainly regulated by monocytes/macrophages, which is closely related to the early inflammation of pyroptosis.

### 2.8 Hub gene immunohistochemistry and cellular localization

The human protein expression profile database provides immunohistochemical analysis and subcellular localization of hub genes in liver cancer-related cells. HMGB1 immunohistochemistry showed that it was mainly expressed in liver cells, and the samples were from patients with liver fibrosis. CYCS immunohistochemistry showed that it was mainly expressed in liver cells and bile duct cells, and the samples were from patients with liver fibrosis. GSDMD immunohistochemistry showed expression in the main bile duct cells, and the samples were from patients with liver fibrosis. IL-1β HE sections showed expression in major liver cells and fibroblasts (HE staining, no immunohistochemical data found). NLRP3 immunohistochemistry shows that it is mainly expressed in liver cells and bile duct cells. IL18 immunohistochemistry showed that it was mainly expressed in bile duct cells (Fig S3 A-F).

### 2.9 Validation of hub genes in hepatocellular Cancer

To further validate the aforementioned results, we employed RT-qPCR, immunohistochemistry, and Western blot to examine the expression of key genes (NLRP3, IL18,

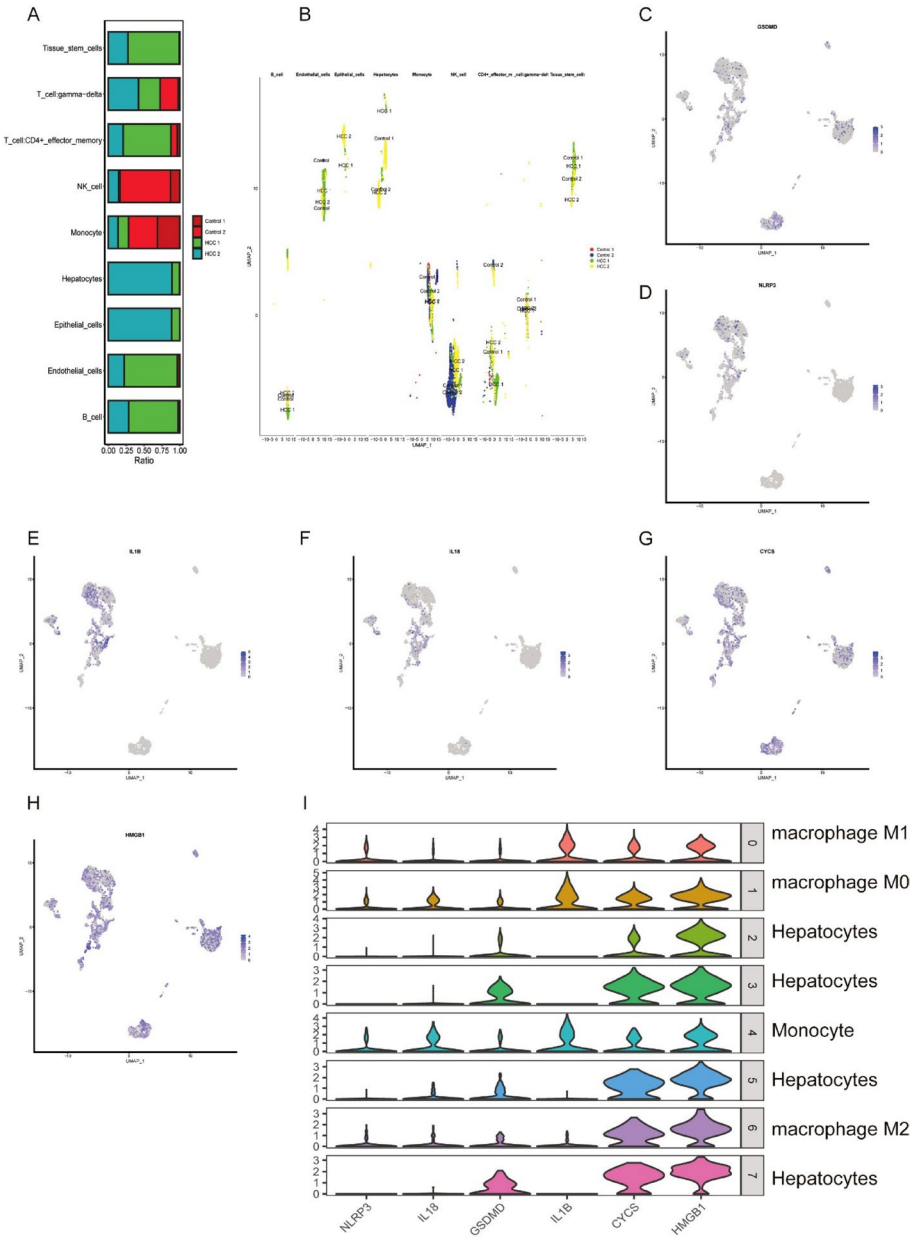


**Fig. 8** Distribution of cell populations and hub genes: **A** heatmap of different cell populations in different tissues, **B** UMAP map of different cells in different tissues, **C** UMAP distribution of GSDMD in the cell population of secondary clustering, **D** UMAP distribution of NLRP3 in the cell population of secondary clustering, **E** IL-1β UMAP distribution in the cell population of secondary clustering. **F** The UMAP distribution of IL18 in the cell population of secondary clustering, the UMAP distribution of **G** CYCS in the cell population of secondary clustering, the UMAP distribution of **H** HMGB1 in the cell population of secondary clustering, and the violin expression map of **I** hub genes in the cell population of secondary clustering

GSDMD, IL-1β, CYCS, and HMGB1) in HCC and paracancerous tissue (PC). We collected cancerous and PC from 10 patients who underwent curative hepatectomy at The Affiliated Traditional Chinese Medicine Hospital, Southwest Medical University. Part of the samples was used for immunohistochemistry, while the remainder was used for protein and RNA extraction for Western blot and RT-qPCR analyses. The RT-qPCR results indicated that the expression levels of pyroptosis-related genes NLRP3 (**$P<0.01$), IL18 (**$P<0.01$), GSDMD (*$P<0.05$), IL-1β (**$P<0.01$), CYCS (*$P<0.05$), and HMGB1

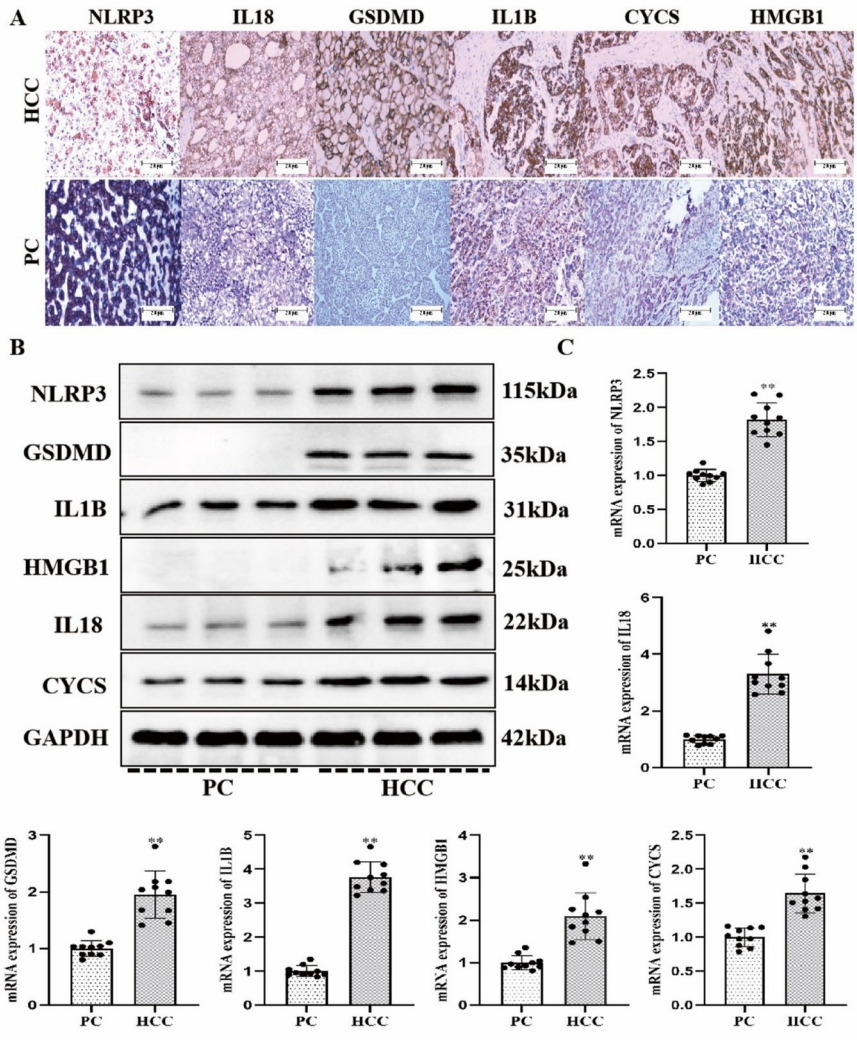


**Fig. 9** Validation of Hub Genes in Hepatocellular Cancer (**A**) Immunohistochemical staining images of cancerous and paracancerous tissue(PC) from HCC patients, with a scale bar of 200 μm ($n=3$). **B** Expression of hub gene mRNA ($n=10$). NLRP3 (**$P<0.01$) vs. PC, IL18 (**$P<0.01$) vs. PC, GSDMD (*$P<0.05$) vs. PC, IL-1β (**$P<0.01$) vs. PC, CYCS (*$P<0.05$) vs. PC, and HMGB1 (**$P<0.01$). **C** Differences in hub gene protein levels between HCC and PC ($n=3$)

(**$P<0.01$) were significantly elevated in HCC tissues compared to PC tissues (Fig. 9B). The results of immunohistochemical staining and Western blot analyses were consistent with those of RT-qPCR; significant upregulation of NLRP3, IL18, GSDMD, IL-1β, CYCS, and HMGB1 was detected in HCC tissues (Fig. 9A-C, Figure S3G). These findings preliminarily validated our previous analyses.

## 3 Discussion

Particularly HCC, liver cancer ranks fourth in the world for cancer-related mortality and is the sixth most frequent cancer globally, placing a heavy load on health care systems. Between 85% and 90% of all initial liver malignancies are HCCs [47]. Even with improvements in adjuvant therapy, liver transplantation, and surgery, the survival rate for people with HCC is still not good enough [48]. Thus, it is still essential to clarify the molecular causes of HCC and find novel treatment targets [24]. A significant concentration of

macrophages has been seen in HCC liver tissue and mouse models, suggesting that liver macrophages play a complex role in the pathophysiology of HCC. These macrophages suppress anti-tumor immunity because they support tumor growth [49]. Liver macrophages secrete pro-angiogenic factors, which together stimulate tumor growth, during the evolution of HCC. These factors include transforming growth factor-β (TGF-β), vascular endothelial growth factor (VEGF), and platelet-derived growth factor (PDGF) [50]. Pyroptosis is a type of programmed cell death linked to inflammation that contributes to the growth of tumors in two distinct manners. On the one hand, pyroptosis induction can stop tumor cells from proliferating and migrating. On the other side, an inflammatory tumor microenvironment (TME), which promotes tumor growth, might result from overactivation of pyroptosis. GSDMD-mediated cell pyroptosis in HCC can activate tumor-infiltrating macrophages, promoting phagocytosis and anti-tumor immunity [51]. It's interesting to note that GSDMD in HCC shows distinct signs of immune cell infiltration. The majority of GSDMDs have a negative correlation with macrophages and a positive correlation with B cells, neutrophils, and dendritic cells. It can be seen that the tumor immune microenvironment, especially macrophages, is closely related to the occurrence and development of cell pyroptosis, but further exploration is needed in HCC. Thus, by combining single-cell technology with bioinformatics, we were able to uncover the mechanism of action of pyroptosis and macrophages in HCC, offering direction for the clinical diagnosis and therapy of HCC.

In this study, we analyzed gene expression between liver cancer tissue and normal tissue adjacent to the cancer using the GEO database, and obtained six HCC related pyroptosis hub genes HMGB1, CYCS, GSDMD, IL-1β, NLRP3, and IL18. Through enrichment analysis, it was determined that the occurrence of HCC is closely associated with signaling pathways such as Necroptosis, Pyroptosis multiple species, NF kappa B signaling pathway, Autophagy animal, Hepatitis C, Hepatitis B, Pyroptosis, Interleukin-18-Signaling INTERLEUKIN_18_SIGNALING, and The-NLRP3-Inflammasome. Through single-cell sequencing data, we found that the main infiltrating cells in liver cancer tissue include NK-cell, Monocyte, T-cell: CD4 + effector memory, Hepatocytes, Endothelial-cells, Tissue_stem-cells, B-cell, Epithelial-cells, Hepatocytes, T-cell: gamma delta, macrophage M1, macrophage M0, macrophage M2. As for HCC itself, it is mainly related to the inflammatory processes of Endothelial cells, Tissue stem cells, Epithelial cells, and Hepatocytes. Regarding the tumor immune microenvironment, it is mainly related to the differentiation and function of NK-cell, Monocyte, T-cell: CD4 + effector_memory, macrophages. The identification of malignant cells further confirms the close relationship between these cells and the progression of cancer. Further analysis of cell trajectories revealed that polarization of monocytes and macrophages first plays a role in HCC. In addition, key apoptotic targets such as HMGB1, CYCS, GSDMD, IL-1β, NLRP3, and IL18 regulate macrophage polarization and affect HCC. Inter cellular communication indicates that the MIF and VEGF signaling pathways are activated in HCC tumors.

Recent studies have shown that HMGB1 is up-regulated in human rectal cancer, breast cancer, cervical cancer, lung cancer and other malignant tumors, which is closely related to the occurrence, growth, invasion and metastasis of tumors, and can be used as a serum marker to provide reference value for tumor progress and prognosis evaluation [52]. A prerequisite for cellular angiogenesis in HCC has been found to be RAGE, whereas HMGB1 is thought to be a pro-angiogenic factor that causes colon carcinoma

to produce VEGF. Given that RAGE is one of HMGB1's receptors, this obliquely implies that HMGB1 may use RAGE to generate angiogenesis in HCC [53]. This time, we found increased expression of HMGB1 in HCC by immunohistochemistry, tissue proteins and RNA, which directly indicates that HMGB1 is a risk factor for HCC. And in single-cell expression, HMGB1 was also expressed in various immune cells and hepatocytes, which again established that HMGB1 contributes to the hepatic microenvironment and the development of HCC. Research has shown that dysregulation of key proteins involved in GSDMD, IL-1β, and NLRP3 pyroptosis may lead to the occurrence and development of various human diseases, particularly malignant tumors [54]. Zhang et al.'s work demonstrated that mifepristone reduces HCC cell growth by pyroptosis that is dependent on BAX-caspase-GSDME, and that the ROS-MEK-ERK1/2 pathway is involved in pyroptosis regulation [55]. Similar research by Yu et al. previously demonstrated that GSDME can promote ROS/JNK/Bax mitochondrial cell pyroptosis pathways and caspase-3/-9 activation in lobaplatin-mediated cell pyroptosis [56]. Our investigation revealed that patients in high-risk groups (liver cancer tissue) not only had cell necrosis but also an accumulation of immune-suppressive cells including macrophages, T cell regulators (Tregs), T cell CD4+, and cancer-related endothelial cells. It is commonly accepted that the infiltration of macrophages in TME results in an immunosuppressive milieu and treatment resistance, both of which are frequently linked to unfavorable prognoses and outcomes [54]. Fatty liver and ECM deposition can result from inflammation associated with chronic liver disease. Fibrous scars will eventually build up and cause cirrhosis if they are not treated, which will result in HCC. The primary constituents of the tumor microenvironment are tumor-associated macrophages, which are highly malleable and can differentiate into M1 and M2 phenotypes, which is crucial for the advancement of HCC. TLR2 ligands in HCC have been shown to decrease NF-κB activity and increase M2 macrophage polarization. Additional investigation reveals that HMGB1 generated from HCC promotes the development of HCC by inducing M2 polarization via the TLR2/NOX2/autophagy axis [17]. Furthermore, angiogenesis is a key aspect of the growth of tumors. Studies have demonstrated that lncRNA CRNDE can stimulate M2 polarization and angiogenesis; its mechanism involves upregulating the expression of proteins associated to angiogenesis, including JAK1, STAT6, AKT1, and others [57]. In conclusion, M1 macrophages perform antigen presentation, pathogen removal, and anti-tumor activities. They also provide protection against viral hepatitis and parasite-induced HCC. On the other hand, M2 macrophages can efficiently treat liver illnesses mostly brought on by inflammatory damage, exhibit anti-inflammatory properties, and aid in wound healing. In our cell trajectory analysis, it also clearly shows that monocytes, M1 macrophages play a role in early cancer defense, and as cancer advances, M2 macrophages gradually appear and play anti-inflammatory effects. These studies directly demonstrate the polarization of M1 to M2 in macrophages in HCC, consistent with existing studies in general. The present study reveals that macrophage polarization in the micro-environment of HCC is characterized by a dynamic temporal sequence: early monocytes/M1-type resist tumors through pro-inflammatory responses (e.g., IL-12 secretion), whereas macrophages are gradually converted to M2-type with the activation of TLR2/HMGB1 signaling and metabolic reprogramming mediated by the STAT6/AKT1 pathway to form an immune-suppressive ecosystem. This polarization dynamics is synergistic with the "inflammation-cancer" process and is spatially heterogeneous

(e.g., M2 enrichment in the hypoxic core). To address this mechanism, targeting TLR2/STAT6 pathway inhibitors, blocking HMGB1, or combining with PD-1 therapies can reverse M2 polarization, while modulation of lncRNA CRNDE or metabolic microenvironment (e.g., lactate/MCT1) can enhance anti-tumor immunity. Future development of spatiotemporal-specific drug delivery systems and balancing the double-edged effects of M1/M2 are needed to achieve precise interventions.

The late stage of hepatocyte pyroptosis, accompanied with the release of inflammatory factors such as IL-1 β and IL-18, is central to the deterioration of hepatocyte cells. Our preliminary experiments also found the expression of the related proteins in HCC. KEGG signaling analysis showed that inflammatory factors released by hepatocyte pyroptosis enhanced the activation of signaling pathways such as NF- κ B, apoptosis, and MAPK in hepatocytes and macrophages, thus further promoting the inflammatory response. Meanwhile, single-cell analysis suggests that the release of proinflammatory factors can recruit mononuclear macrophages in vivo, leading to a more severe inflammatory response and ultimately massive hepatocyte death. Moreover, several studies have shown that there is a reciprocal regulation between macrophage polarization and pyroptosis. Therefore, we believe that the regulation of macrophage polarization and pyroptosis in hepatocytes will be a new therapeutic direction. In this study, we also have some deficiencies and challenges. First, the number of samples verified for clinical tissues is limited, so the credibility of the data needs to be improved. Among them, we only verified the key hub genes, and the mechanism of the related signaling pathways needs many experiments to prove. Of course, this study is still of clinical significance. First of all, we initially found that pyroptosis-related memory and immune cells, especially macrophages, are one of the pathogenesis of HCC, which will provide a direction for future clinical research.

## 4 Conclusion

In conclusion, we initially found the disease molecular mechanism of HCC, and the main molecular mechanism of the pathogenesis process is immune cell infiltration, especially macrophage polarization promotes inflammatory factor secretion leading to pyroptosis. We finally speculate that hub genes such as HMGB1, CYCS, GSDMD, IL1B, NLRP3 and IL 18 are the links for the development of macrophage polarization and pyroptosis during HCC, and we will further elucidate the roles of these genes, including functional experiments (e.g., in vitro macrophage-pyroptosis assays) in future work.

[.

## Supplementary Information

The online version contains supplementary material available at https://doi.org/10.1007/s12672-025-02907-3.

Figure S1 single-cell sample RNA expression data: a sample RNA scatter plot, a sample RNA violin plot

Figure S2 Cell Filtration and Batch Removal: a. Single Cell Sample PC Scatter Plot, b. Single Cell Sample PC Curve Plot, c. RNA Violin Plot after Single Cell Sample Filtration, d. UMAP Plot before Batch Removal of Single Cell Samples, e. Harmony Batch Quality Control, f. UMAP Plot after Batch Removal of Single Cell Samples

Figure S3 Histochemistry of Hub Genes: A Exemption from immunohistochemistry for HMGB1, B. CYCS, C. GSDMD, D. IL-1β HE staining, E. NLRP3, and F.IL18. G.Gray scale values of Hub Genes

Supplementary Table S1 Patient clinical information. Supplementary Table S2 GSE46408 Sample Tissue Expression Profile Data Supplementary Table S3 GSE46408 Sample Tissue Differential Gene Expression Profile Supplementary Table S4 Cellular pyroptosis gene data Supplementary Table S5 Forest Pattern Prediction Genes Supplementary Table S6 Expression data of liver cancer necrosis characteristic genes Supplementary Table S7 Single cell marker gene data

Supplementary Material 5

**Acknowledgements**
We thank the CEO (Home - GEO - NCBI https://www.ncbi.nlm.nih.gov/geo) database for providing the underlying data for this study and all the patients and families who provided clinical samples for this study.

**Author contributions**
Conceptualization, Methodology, Data analysis, Writing - original draft: W. Lou and J.X. Wang; Images analysis, Providing technical support, Performing the experiments: H.F. Wang, T.W. Yang and F. Liu; Conceptualization, Supervision, Funding, Writing – review & editing: Z.J. Wu andW.B. Guo; All authors participated in these experiments.

**Funding**
The following grants supported this work: The Science and Technology Project of Sichuan Provincial Administration of Traditional Chinese Medicine (Nos. 2024MS151), The Southwest Medical University Integrated Traditional Chinese and Western Medicine Special Project (Nos. 2023ZYYJ07), and The Joint Project of Southwest Medical University and Affiliated Traditional Chinese Medicine Hospital of Southwest Medical University (Nos. 2020XYLH- 021).

**Data availability**
All data generated or analyzed during this study are included in this published article.

## Declarations

**Ethics approval and consent to participate**
The studies involving humans were approved by the Ethics Committee of The Affiliated Traditional Chinese Medicine Hospital, Southwest Medical University (Nos. YJ-KY2024048). The studies were conducted in accordance with the local legislation and institutional requirements. The patients provided their written informed consent to participate in this study.

**Competing interests**
The authors declare no competing interests.

Received: 26 December 2024 / Accepted: 4 June 2025
Published online: 14 June 2025

**References**

1. Jemal A et al. *Annual Report to the Nation on the Status of Cancer, 1975–2014, Featuring Survival.* J Natl Cancer Inst, 2017. 109(9).
2. Alvarez M, et al. Human liver single nucleus and single cell RNA sequencing identify a hepatocellular carcinoma-associated cell-type affecting survival. Genome Med. 2022;14(1):50.
3. Piñero F, Dirchwolf M, Pessôa MG. Biomarkers in hepatocellular carcinoma: diagnosis, prognosis and treatment response assessment. Cells, 2020. 9(6).
4. Sung H, et al. Global Cancer statistics 2020: GLOBOCAN estimates of incidence and mortality worldwide for 36 cancers in 185 countries. CA Cancer J Clin. 2021;71(3):209–49.
5. Refolo MG et al. Inflammatory mechanisms of HCC development. Cancers (Basel), 2020. 12(3).
6. Nevola R, et al. Predictors of early and late hepatocellular carcinoma recurrence. World J Gastroenterol. 2023;29(8):1243–60.
7. Massalha H, et al. A single cell atlas of the human liver tumor microenvironment. Mol Syst Biol. 2020;16(12):e9682.
8. Ma L, et al. Single-cell atlas of tumor cell evolution in response to therapy in hepatocellular carcinoma and intrahepatic cholangiocarcinoma. J Hepatol. 2021;75(6):1397–408.
9. Craig AJ, et al. Tumour evolution in hepatocellular carcinoma. Nat Rev Gastroenterol Hepatol. 2020;17(3):139–52.
10. Guerra F et al. Mitochondria-Derived vesicles, sterile inflammation, and pyroptosis in liver cancer: partners in crime or innocent bystanders?? Int J Mol Sci, 2024. 25(9).
11. Deng M, et al. The pyroptosis-related gene signature predicts prognosis and indicates immune activity in hepatocellular carcinoma. Mol Med. 2022;28(1):16.
12. Zou Z, et al. The role of pyroptosis in hepatocellular carcinoma. Cell Oncol (Dordr). 2023;46(4):811–23.
13. Zhang L, et al. Pyroptosis in liver disease. Rev Esp Enferm Dig. 2021;113(4):280–5.
14. Cheng C, et al. Burning down the house: pyroptosis in the tumor microenvironment of hepatocellular carcinoma. Life Sci. 2024;347:122627.
15. Aizawa S, Brar G, Tsukamoto H. Cell death and liver disease. Gut Liver. 2020;14(1):20–9.
16. Stoess C et al. Cell death in liver disease and liver surgery. Biomedicines, 2024. 12(3).
17. Wang C, et al. Macrophage polarization and its role in liver disease. Front Immunol. 2021;12:803037.
18. Napodano C et al. NLRP3 inflammasome involvement in heart, liver, and lung Diseases-A lesson from cytokine storm syndrome. Int J Mol Sci, 2023. 24(23).
19. Hou J, et al. PD-L1-mediated gasdermin C expression switches apoptosis to pyroptosis in cancer cells and facilitates tumour necrosis. Nat Cell Biol. 2020;22(10):1264–75.
20. Xing M, Li J. Diagnostic and prognostic values of pyroptosis-related genes for the hepatocellular carcinoma. BMC Bioinformatics. 2022;23(1):177.
21. Jiao Y et al. Icaritin exerts Anti-Cancer effects through modulating pyroptosis and immune activities in hepatocellular carcinoma. Biomedicines, 2024. 12(8).

22. Yu W, et al. Myeloid Trem2 ameliorates the progression of metabolic dysfunction-associated steatotic liver disease by regulating macrophage pyroptosis and inflammation resolution. Metabolism. 2024;155:155911.
23. Ni L, et al. Unveiling the flames: macrophage pyroptosis and its crucial role in liver diseases. Front Immunol. 2024;15:1338125.
24. Finotto S, et al. Severe hepatic injury in Interleukin 18 (IL-18) Transgenic mice: a key role for IL-18 in regulating hepatocyte apoptosis in vivo. Gut. 2004;53(3):392–400.
25. Huang J, et al. Macrophage metabolism, phenotype, function, and therapy in hepatocellular carcinoma (HCC). J Transl Med. 2023;21(1):815.
26. Song X, et al. Identification of potential hub genes related to the progression and prognosis of hepatocellular carcinoma through integrated bioinformatics analysis. Oncol Rep. 2020;43(1):133–46.
27. Shen W, et al. Sangerbox: A comprehensive, interaction-friendly clinical bioinformatics analysis platform. iMeta. 2022;1(3):e36.
28. Song C, et al. Bioinformatics-based discovery of intervertebral disc degeneration biomarkers and immune-inflammatory infiltrates. JOR Spine. 2024;7(1):e1311.
29. Song C, et al. Single-Cell analysis integrated with machine learning elucidates the mechanisms of nucleus pulposus cells apoptosis in intervertebral disc degeneration and therapeutic interventions. JOR Spine. 2025;8(1):e70036.
30. Liberzon A, et al. The molecular signatures database (MSigDB) hallmark gene set collection. Cell Syst. 2015;1(6):417–25.
31. Zhang Y, et al. Finding key genes (UBE2T, KIF4A, CDCA3, and CDCA5) co-expressed in hepatitis, cirrhosis and hepatocellular carcinoma based on multiple bioinformatics techniques. BMC Gastroenterol. 2024;24(1):205.
32. Ganggayah MD, et al. Predicting factors for survival of breast cancer patients using machine learning techniques. BMC Med Inf Decis Mak. 2019;19(1):48.
33. Asner GP, et al. Airborne laser-guided imaging spectroscopy to map forest trait diversity and guide conservation. Science. 2017;355(6323):385–9.
34. Lu Y, et al. M2 macrophage-secreted exosomes promote metastasis and increase vascular permeability in hepatocellular carcinoma. Cell Commun Signal. 2023;21(1):299.
35. Kanehisa M, Goto S. KEGG: Kyoto encyclopedia of genes and genomes. Nucleic Acids Res. 2000;28(1):27–30.
36. Kanehisa M, et al. KEGG: new perspectives on genomes, pathways, diseases and drugs. Nucleic Acids Res. 2017;45(D1):D353–61.
37. Szklarczyk D, et al. The STRING database in 2021: customizable protein-protein networks, and functional characterization of user-uploaded gene/measurement sets. Nucleic Acids Res. 2021;49(D1):D605–12.
38. Otasek D, et al. Cytoscape automation: empowering workflow-based network analysis. Genome Biol. 2019;20(1):185.
39. Sun BY, et al. Dissecting Intra-Tumoral changes following immune checkpoint Blockades in intrahepatic cholangiocarcinoma via Single-Cell analysis. Front Immunol. 2022;13:871769.
40. Liang J et al. Single-cell transcriptomics analysis reveals intratumoral heterogeneity and identifies a gene signature associated with prognosis of hepatocellular carcinoma. Biosci Rep, 2022. 42(2).
41. Huang LL. Interpersonal harmony and conflict for Chinese people: A Yin-Yang perspective. Front Psychol. 2016;7:847.
42. Su Z, et al. Coupled scRNA-seq and Bulk-seq reveal the role of HMMR in hepatocellular carcinoma. Front Immunol. 2024;15:1363834.
43. Liu F, et al. Unraveling the enigma of B cells in diffuse large B-cell lymphoma: unveiling cancer stem cell-like B cell subpopulation at single-cell resolution. Front Immunol. 2023;14:1310292.
44. Ni L, et al. The expression and prognostic value of Disulfidptosis progress in lung adenocarcinoma. Aging. 2023;15(15):7741–59.
45. Boopathi S, et al. Intercellular communication and social behaviors in mycobacteria. Front Microbiol. 2022;13:943278.
46. Bastians H, Ponstingl H. The novel human protein serine/threonine phosphatase 6 is a functional homologue of budding yeast Sit4p and fission yeast ppe1, which are involved in cell cycle regulation. J Cell Sci. 1996;109(Pt 12):2865–74.
47. Zou H, et al. Economic burden and quality of life of hepatocellular carcinoma in greater china: A systematic review. Front Public Health. 2022;10:801981.
48. Raffetti E, et al. Is survival for hepatocellular carcinoma increasing? A population-based study on survival of hepatocellular carcinoma patients in the 1990s and 2000s. Clin Res Hepatol Gastroenterol. 2021;45(1):101433.
49. Ding T, et al. High tumor-infiltrating macrophage density predicts poor prognosis in patients with primary hepatocellular carcinoma after resection. Hum Pathol. 2009;40(3):381–9.
50. Ju C, Tacke F. Hepatic macrophages in homeostasis and liver diseases: from pathogenesis to novel therapeutic strategies. Cell Mol Immunol. 2016;13(3):316–27.
51. Zhang Z, et al. Gasdermin E suppresses tumour growth by activating anti-tumour immunity. Nature. 2020;579(7799):415–20.
52. Wen S, et al. HMGB1-associated necroptosis and Kupffer cells M1 polarization underlies remote liver injury induced by intestinal ischemia/reperfusion in rats. Faseb J. 2020;34(3):4384–402.
53. Wang X, et al. The role of HMGB1 signaling pathway in the development and progression of hepatocellular carcinoma: A review. Int J Mol Sci. 2015;16(9):22527–40.
54. Chen X, et al. Identification and in vitro and in vivo validation of the key role of GSDME in pyroptosis-related genes signature in hepatocellular carcinoma. BMC Cancer. 2023;23(1):411.
55. Zhang X, et al. Miltirone induces cell death in hepatocellular carcinoma cell through GSDME-dependent pyroptosis. Acta Pharm Sin B. 2020;10(8):1397–413.
56. Yu J, et al. Cleavage of GSDME by caspase-3 determines lobaplatin-induced pyroptosis in colon cancer cells. Cell Death Dis. 2019;10(3):193.
57. Hou ZH, et al. Long non-coding RNA MALAT1 promotes angiogenesis and immunosuppressive properties of HCC cells by sponging miR-140. Am J Physiol Cell Physiol. 2020;318(3):C649–63.


## Publisher's note